energy&fuels

pubs.acs.org/EF

Article

Revisiting Reaction Kinetics of CO Electroreduction to C_{2+} Products in a Flow Electrolyzer

Published as part of Energy & Fuels virtual special issue "2023 Energy and Fuels Rising Stars".

Zhengyuan Li, Tianyu Zhang, Jithu Raj, Soumyabrata Roy, and Jingjie Wu*

Cite This: *Energy Fuels* 2023, 37, 7904–7910

Read Online

ACCESS | Metrics & More | Article Recommendations | Supporting Information

ABSTRACT: The identification of the rate-determining step (RDS) in the electrochemical CO/CO_2 reduction to multi-carbon (C_{2+}) products has been complicated by the deficiency of rigorous reaction kinetic data. This work describes an experimental analysis of the key reaction steps by exploring the effect of CO partial pressure on the activity of C_{2+} products. With the aid of a flow electrolyzer integrated with a gas diffusion electrode, the distinct reaction orders of CO and reaction mechanisms in forming different C_{2+} products were determined. Specifically, *CO dimerization is identified as the RDS for ethylene and ethanol production, as evidenced by the gradual transition of measured CO reaction order from second to zero as CO partial pressure increases from 0.05 to 1 atm. The formation of *n*-propanol is suggested to proceed *via* the *CO trimerization mechanism. The acetate generation mechanism might involve a critical step of *CO hydrogenation before C−C coupling. Kinetic studies reveal that product-specific active sites are responsible for activity and selectivity toward specific C_{2+} products over oxide-derived copper.

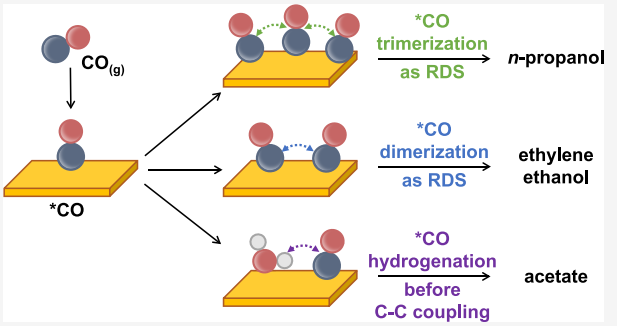

1. INTRODUCTION

Electrochemical CO_2 reduction reaction (CO_2RR) provides potential pathways for closing the carbon loop with sustainable chemical production.[1] Copper (Cu)-based catalysts have attracted much attention since their unique intermediate adsorption strength delivers high-value multi-carbon (C_{2+}) products.[1,2] The understanding of the reaction mechanism, especially identification of the rate-determining step (RDS), is crucial to the rational design of advanced catalysts with enhanced C_{2+} product selectivity.[3] So far, most mechanistic studies invoke three main RDSs leading to C_{2+} production and are as follows: (i) dimerization of two adsorbed CO (*CO), (ii) dimerization of one *CO with one gaseous CO ($CO_{(g)}$), and (iii) protonation of *CO to *CO(H).[4−9] However, the elucidation of plausible reaction pathways increasingly relies on theoretical computations due to the limited availability of reliable kinetic datasets from rigorous experiments.

In addition to the direct CO_2 electrolysis, electrocatalytic CO reduction reaction (CORR) has been increasingly explored, given the key role of CO as an intermediate for C−C coupling.[10,11] CORR is an advantageous proxy in the mechanistic study of CO_2RR since it circumvents the complexity of multiple equilibria between CO_2 and the local alkaline environment.[12] Prior studies on the microkinetic analyses for CORR in the H-cell drew inconsistent conclusions regarding CO reaction orders and RDSs of C_{2+} production.[13−16] Some studies suggested that the RDS for the formation of C_{2+} products proceeded *via* two *CO couplings following the Langmuir−Hinshelwood mechanism, deriving from CO reaction order, Tafel slope, pH effect, and kinetic isotope effect.[13,16] On the contrary, a recent study revealed the RDS of C_{2+} products to be *CO hydrogenation with adsorbed water (H_2O_{ad}) by employing *in situ* surface-enhanced infrared absorption spectroscopy to determine the CO adsorption isotherms.[15] However, this hypothesis failed to interpret the pH-independent activity of C_{2+} product formation in acidic conditions. Additionally, several limitations exist in the above experiments. For instance, (i) kinetic data were compared under only one potential. (ii) CO conversion was not carefully controlled, which is essential for reaction order determination. (iii) Insufficient data were collected in the low CO partial pressure (P_{CO}) region owing to the sluggish reaction rate in the H-cell. (iv) All C_{2+} products were considered in general, rather than discussing each product individually.

The low solubility of CO in aqueous electrolytes (~1.0 mM under ambient conditions) constrains the potential window

Received: March 5, 2023
Revised: April 27, 2023
Published: May 19, 2023

over which activation-controlled CO reduction kinetics can be probed in the H-cell.[13] When conducting kinetic investigations relative to P_{CO}, rigorous experimental design and product quantification must be emphasized. To this end, the gas diffusion electrode (GDE)-based flow cell offers a more reliable platform for conducting P_{CO}-dependent experiments. The construction of the triple-phase interface in the GDE-based flow cell could circumvent the gaseous CO transport limitation, enabling more precise measurements under industrial relevant conditions. Meanwhile, the high surface area-to-volume ratio of the GDE provides a large number of active sites, compared to traditional foil electrodes, which improves reaction kinetics at the lowest possible P_{CO}.

Herein, we explore the RDSs of CORR to C_{2+} products on the GDE incorporating oxide-derived Cu nanoparticles (NPs). The reaction order of CO was first determined by adjusting P_{CO} in a flow electrolyzer under varying potentials. After that, the Langmuir adsorption isotherm was applied to fit the data to verify and identify RDSs that were theoretically derived. The activity of different C_{2+} products was found to be limited by distinct key elementary steps on product-specific active sites. The RDS of ethylene (C_2H_4) and ethanol (C_2H_5OH) is identified to be *CO dimerization. The *n*-propanol (C_3H_7OH) formation probably proceeds through the *CO trimerization mechanism. The *CO protonation before C−C coupling is proposed to be a critical step invoking acetate (CH_3COO^-) production. Our findings illustrate the feasibility of using facile kinetic experiments to understand the key reaction steps that govern the formation of C_{2+} products from $CO_{(2)}$RR.

2. EXPERIMENTAL SECTION

2.1. Catalyst Synthesis and Characterizations. CuO NPs were prepared by a pH-controlled precipitation method. Sodium bicarbonate (0.5 M, Na_2CO_3, Sigma-Aldrich) was progressively added into copper(II) chloride dihydrate (0.5 M, $CuCl_2{\cdot}2H_2O$, Sigma-Aldrich) under strong stirring until pH 10. The mixture was aged at 60 °C for 16 h and then collected by wash and centrifugation. After drying at 60 °C overnight, the sample was annealed at 300 °C for 5 h to obtain CuO NPs. The oxide-derived Cu catalyst was obtained *via in situ* electroreduction of CuO under CORR conditions.

Transmission electron microscopy (TEM) characterization was performed on a JEOL JSM-2010F. X-ray photoelectron spectroscopy (XPS) data was collected from the PHI Quantera XPS with the Al Kα X-ray source. X-ray diffraction (XRD) was carried out on a Rigaku D/Max Ultima II configured with Cu Kα radiation.

2.2. Electrocatalytic Measurements. The CORR performance was measured in a customized flow cell with 1 M KOH as the electrolyte. The cathode GDE was prepared by the air-brushing method. The mass loading of CuO NPs was ∼0.25 mg cm^{-2}. A nickel foam was used as the anode. An anion exchange membrane (FAA-3-PK-130) was used to separate cathodic and anodic compartments. The electrolyte was fed by syringe pumps (New Era Pump Systems Inc.) at 5 and 10 mL min^{-1} to the cathode and anode chambers, respectively. The CO/Ar gas mixture with different P_{CO} (0.05−1 atm) was supplied to the cathode at 80 sccm *via* mass flow controllers (Alicat Scientific). A potentiostat (Gamry Interface 1010E) controlled a constant voltage to the flow cell and recorded the corresponding current. The cathode potential was measured relative to the Ag/AgCl (3 M KCl) reference electrode. All potentials were converted to the RHE scale using $E_{RHE} = E_{Ag/AgCl} + 0.209\ V + 0.0591 \times pH$. The iR compensation was performed by potentiostatic electrochemical impedance spectroscopy (EIS). During the electrolysis, an on-line gas chromatograph (GC, SRI Instruments Multiple Gas #5) equipped with both a thermal conductivity detector and a flame ionization detector was used to monitor the gas products. The liquid products after electrolysis were quantified *via* ^{1}H NMR (Bruker AV 400 MHz spectrometer). The electrolyte (500 μL) was mixed with a 100 μL internal standard of 5 mM 3-(trimethylsilyl)propionic-2,2,3,3-d_4 acid sodium salt in D_2O.

3. RESULTS AND DISCUSSION

3.1. P_{CO}-Dependent Activity of C_{2+} Product Formation on Oxide-Derived Cu. The oxide-derived Cu catalyst was synthesized through *in situ* reduction of CuO NPs under CORR conditions (Figures S1 and S2). The TEM images show abundant grain boundaries on the catalyst surface (Figure 1), which were identified as the most active sites for

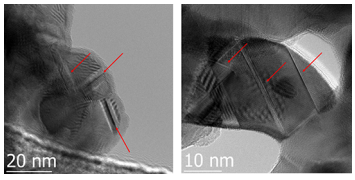

Figure 1. TEM images of the oxide-derived Cu catalyst. The red arrows denote surface defects, such as grain boundaries.

CO-to-C_{2+} product conversion.[17,18] The CORR performance was evaluated in a flow cell with a 1 M KOH electrolyte. The P_{CO} was varied from 0.05 to 1 atm by balancing the total pressure with an inert Ar gas. A high gaseous flow rate was supplied to ensure a low CO conversion in the flow cell (Table S1), acting as a differential reactor to gain kinetic data. Major C_{2+} products were recorded, including C_2H_4, C_2H_5OH, CH_3COO^-, and C_3H_7OH. Both the Faradaic efficiency (FE) and partial current density (j) for C_{2+} products increase with P_{CO} (Figures S3 and S4). Tafel slopes for C_{2+} products are ∼148 ± 20 mV dec^{-1} (Figures S5−S7), corresponding to a transfer coefficient (α) of ∼0.40 ± 0.05, which generally indicates that the first one-electron transfer process limits the reaction rate.[13,14] In addition, the linear dependence of log(j) on potential suggests the absence of mass transport limitation at potentials between approximately −0.40 and −0.60 V (vs RHE, thereafter) within the investigated P_{CO} range, which meets the pre-requirements for rigorous CO reaction order determination.

3.2. Determination of CO Reaction Order and RDS for C_2H_4 and C_2H_5OH Formation. The dependence of each C_{2+} product activity on P_{CO} is compared at −0.45, −0.50, −0.55, and −0.60 V, derived from the polarization curves in Figure S4. Non-linear relationships of log(j) vs log(P_{CO}) are observed for C_2H_4 and C_2H_5OH products (Figures 2 and 3), indicating that the reaction order of CO may vary with P_{CO}. The reaction order of CO is determined by the slope of every segment of two adjacent points in log(j) vs log(P_{CO}) plots. The reaction order of CO is roughly equivalent to 2 at P_{CO} < 0.0625 atm. The CO reaction order decreases progressively to ∼1 as P_{CO} rises to ∼0.125 atm and approximates to 0 at P_{CO} > 0.5 atm. The second-order reaction at low P_{CO} indicates that CO dimerization (e.g., $CO + CO + e^- \rightarrow C_2O_2^-$) could be the RDS for C_2H_4 and C_2H_5OH formation, validating the previous computational predictions.[4,5] The plateau at higher P_{CO} is caused by a near-saturation surface coverage of adsorbed *CO.[13] A P_{CO} of ∼0.5 atm is inferred as the inflection point at which *CO surface coverage (θ_{CO}) approaches saturation on our oxide-derived Cu catalyst surface. Given that C_2H_4 and C_2H_5OH are the dominant products, the log(j_{C2+}) vs log(P_{CO}) plots of overall C_{2+} products follow similar trends as discussed

https://doi.org/10.1021/acs.energyfuels.3c00736
Energy Fuels 2023, 37, 7904−7910

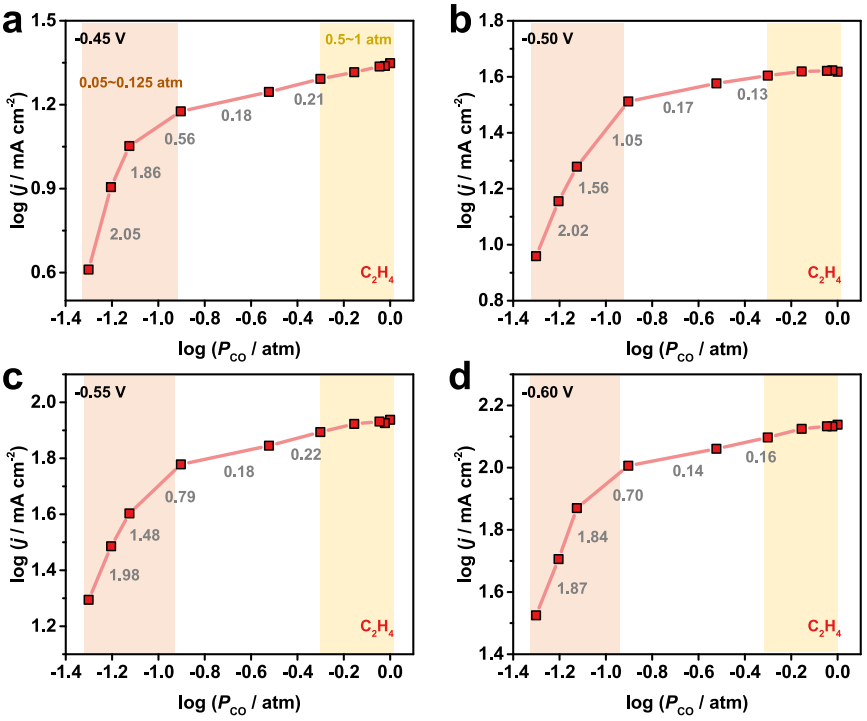

Figure 2. Logarithms of j_{C2H4} vs logarithms of P_{CO} at (a) −0.45 V, (b) −0.50 V, (c) −0.55 V, and (d) −0.60 V. The slopes are next to the line segments between two adjacent data points.

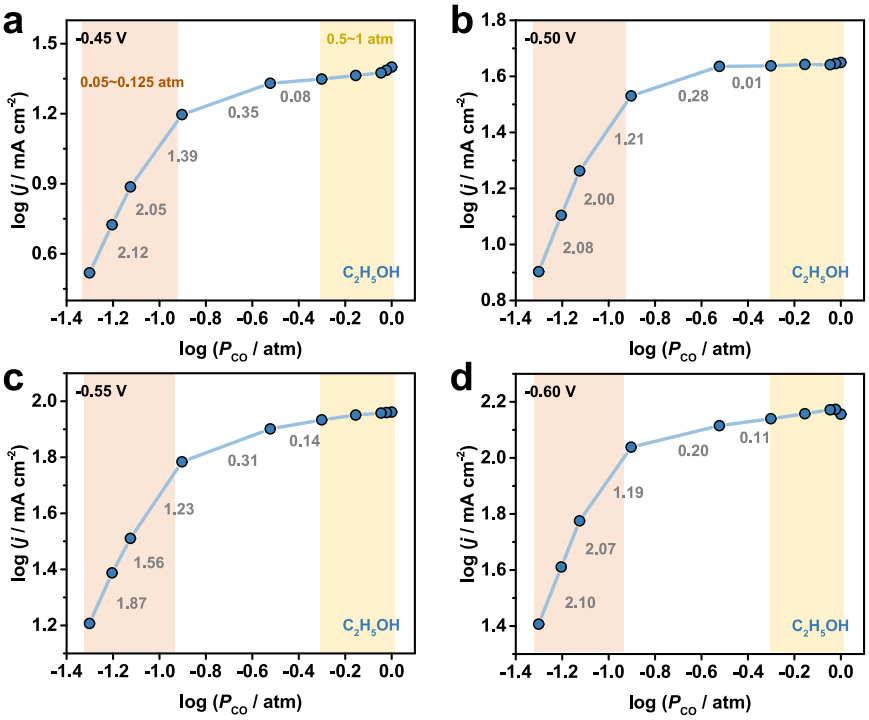

Figure 3. Logarithms of j_{C2H5OH} vs logarithms of P_{CO} at (a) −0.45 V, (b) −0.50 V, (c) −0.55 V, and (d) −0.60 V. The slopes are next to the line segments between two adjacent data points.

above (Figure S8). While probing the reaction mechanism for each specific product, the detailed kinetic analysis for C_3H_7OH and CH_3COO^- is necessary.

The shift from second-order to zero-order reaction as P_{CO} increases indicates that the adsorption of *CO on the catalyst surface plays an important role in the reaction mechanism. Therefore, θ_{CO} should be a more pertinent descriptor to evaluate P_{CO}-dependent activity of C_2H_4 and C_2H_5OH formation. The Langmuir adsorption isotherm is thus applied to obtain a mechanistic interpretation of the surface reactions.[13,19] Specifically, the zero-order reaction at high P_{CO} implies the Langmuir−Hinshelwood (L-H) mechanism for the formation of C_2H_4 and C_2H_5OH since the reaction order of CO should be no less than unity in the Eley−Rideal

https://doi.org/10.1021/acs.energyfuels.3c00736
Energy Fuels 2023, 37, 7904−7910

Table 1. Proposed Reaction Schemes and Rate Laws Assuming CO Dimerization as the RDS for Forming C_2 Products

step	proposed reaction scheme	rate expression[a]	P_{CO}	CO reaction order
L-H mechanism	$*CO + *CO + e^- \rightarrow *C_2O_2^- + *$	$j_{C2} = k_1^0\left(\frac{K_{CO}P_{CO}}{1+K_{CO}P_{CO}}\right)^2 \exp\left(\frac{-\alpha\eta F}{RT}\right)$	low	second
			high	zero
E-R mechanism	$*CO + CO_{(g)} + e^- \rightarrow *C_2O_2^- + *$	$j_{C2} = k_2^0\frac{K_{CO}P_{CO}^2}{1+K_{CO}P_{CO}}\exp\left(\frac{-\alpha\eta F}{RT}\right)$	low	second
			high	first

[a] j_{C2} is the partial current density of a single C_2 product; k^0 is the standard forward rate constant; K_{CO} is the equilibrium adsorption constant for CO; P_{CO} is the partial pressure of CO; α is the transfer coefficient; η is the overpotential for the cathodic reaction; F is the Faraday constant; R is the ideal gas constant; T is the absolute temperature.

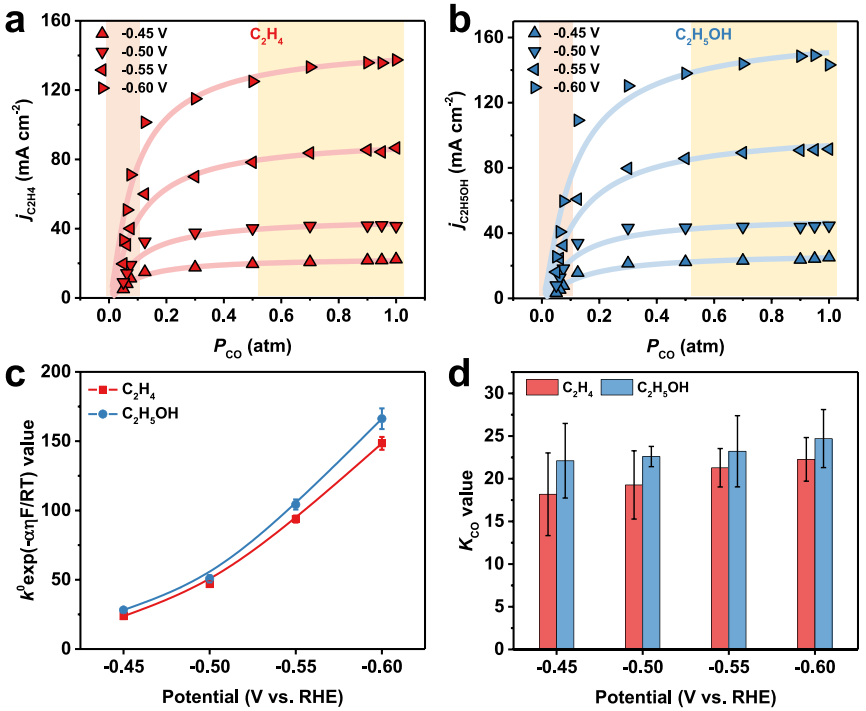

Figure 4. Langmuir isotherm fitting at varying potentials for (a) C_2H_4 and (b) C_2H_5OH. Comparison of (c) values of $k^0\exp\left(\frac{-\alpha\eta F}{RT}\right)$ and (d) values of K_{CO} for C_2H_4 and C_2H_5OH.

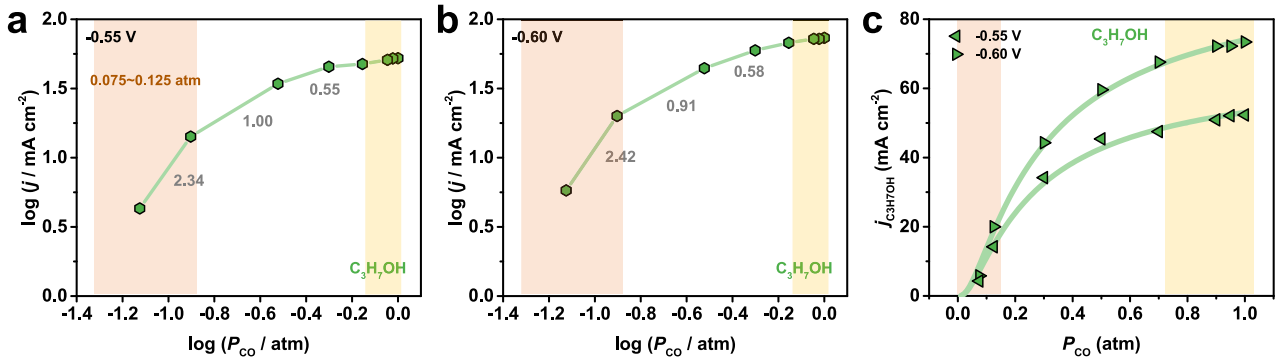

Figure 5. Logarithms of j_{C3H7OH} vs logarithms of P_{CO} at (a) −0.55 V and (b) −0.60 V. The slopes are next to the line segments between two adjacent data points. (c) Langmuir isotherm fitting for C_3H_7OH.

(E-R) mechanism (Table 1, see detailed derivation in the Supporting Information). Indeed, the L-H model fits well with the experimental data on the relationship of C_2H_4/C_2H_5OH formation rate vs P_{CO} at different potentials (Figure 4). Analogous kinetic trends with respect to P_{CO} indicate that the C_2H_4 and C_2H_5OH likely share the same RDS. The selectivity-determining step to a single C_2 product occurs at a late stage after *CO dimerization, in agreement with theoretical studies.[10,11] Two important parameters, rate constant (k^0) and *CO adsorption equilibrium constant (K_{CO}), could be obtained based on fitting results of the L-H mechanism. The value of $k^0\exp\left(\frac{-\alpha\eta F}{RT}\right)$ increases with potential (Figure 4c) as the activation energy barrier of *CO dimerization is lowered.[20] The $k^0\exp\left(\frac{-\alpha\eta F}{RT}\right)$ values of C_2H_5OH are slightly larger than

https://doi.org/10.1021/acs.energyfuels.3c00736
Energy Fuels 2023, 37, 7904−7910

those of C_2H_4 in CORR on our oxide-derived Cu catalyst because high θ_{CO} and low *H coverage enhance the formation of C_{2+} oxygenates over alkene.[20,21] In the Langmuir isotherm, the adsorption equilibrium constant (K) is correlated to the enthalpy of adsorption,[19] which can be used to estimate the relative adsorbate binding strength. The larger the measured K value, the stronger the molecule bound on the surface. The different values of K_{CO} for C_2H_4 and C_2H_5OH reveal that oxide-derived Cu has product-specific active sites responsible for each specific C_2 selectivity.[22,23] In particular, C_2H_5OH-favorable active sites possess stronger *CO binding strength than that for C_2H_4 formation (Figure 4d). These experimental findings support computational results that the C_2H_5OH formation is preferred on high-uncoordinated sites (e.g., steps and kinks), binding *CO stronger than terraces.[23,24]

3.3. Discussion of CO Reaction Order and RDS for C_3H_7OH Formation. The CO reaction order of C_3H_7OH production was estimated to be ~2.4 at P_{CO} between 0.075 and 0.125 atm (Figure 5). Due to the relatively low formation rate, the detection and quantification of C_3H_7OH cannot be reliably conducted at more positive potentials or lower CO pressures (Figure S9). Despite a less rigorous extrapolation, we speculate a third-order reaction for CO at P_{CO} lower than 0.075 atm according to the logarithmic scale trends of C_2H_4 and C_2H_5OH in Figures 3 and 4. The CO reaction order in C_3H_7OH formation gradually decreases to 0 as P_{CO} increases to 0.7 atm. The reaction mechanism for C_3H_7OH formation is more complex and less investigated than those for C_2H_4 and C_2H_5OH formation. The multi-step sequential C−C coupling reactions were proposed, involving initial C_1-C_1 coupling and subsequent C_1-C_2 coupling.[11,25] Our kinetic analysis indicates that a one-step concerted trimerization of *CO to form a key C_3 intermediate is a plausible RDS directing C_3H_7OH formation,[26] which is further supported by the good L-H model fitting results (Figure 5c, see detailed derivation in the Supporting Information). The value of K_{CO} obtained from the L-H model (Figure S10) reveals relatively weaker CO binding on C_3 active sites compared to C_2H_4- and C_2H_5OH-generating sites. Weaker CO binding might contribute to improving long carbon-chain formation *via* such a *CO trimerization mechanism.[26]

3.4. Reaction Mechanism for CH_3COO^- Formation. Distinguished from other C_{2+} products in logarithmic scale plots, the $\log(j_{CH3COO-})$ exhibits a linear relation with $\log(P_{CO})$ at 0.05−0.7 atm with a slope of 1 (Figure 6), indicating a first-order reaction of CO, consistent with prior electrokinetic reports.[27,28] The zero-order dependence occurring at higher P_{CO} (>0.7 atm) is probably attributed to the lower CORR activity to CH_3COO^- over our oxide-derived Cu catalyst than other CH_3COO^--selective catalysts.[28] Some previous studies proposed that the first and zero dependence at low and high P_{CO}, respectively, originated from the coupling between the *CO and *CO(H) intermediate in CH_3COO^- formation.[28,29] However, our derivations show that the reaction order of CO should be 2 at the low P_{CO} region by following such asymmetric C−C coupling (see derivations in the Supporting Information). Xu and co-workers presented the *CO hydrogenation with H_2O_{ad} as the RDS under an unsaturated θ_{CO} condition in an H-cell, which could also interpret our observed P_{CO}-dependent activity.[15] However, kinetic analysis of C_2H_4 and C_2H_5OH, as discussed in Table 1 and Figure 4, suggests that a near-saturated θ_{CO} should be reached in the GDE-based flow cell. It is worth noting that the reaction environment, including pH and mass transport, may play a more significant role than the intrinsic activity of a catalyst when a solution reaction of ketene with OH^- is regarded as the selectivity-determining step toward CH_3COO^-, as evidenced by the positive correlation between CH_3COO^- formation rate and KOH concentration.[30,31] In such a scenario, experimental kinetic analysis by varying P_{CO} only is hard to unravel the possible reaction pathways of CH_3COO^- formation entirely.[31] Taking the above findings and discussion together, we posit that the reaction mechanism of CH_3COO^- formation likely involves the CO hydrogenation step (e.g., $*CO + H_2O + e^- \rightarrow *CO(H) + OH^-$) before the C−C coupling, despite the ambiguous RDS and strong influence from the dynamic local environment. The distinct trends of P_{CO}-dependent activity for CH_3COO^- vs other C_{2+} products suggest that peculiar models are required to guide the design of catalysts or reaction environments for promoting CH_3COO^- selectivity.

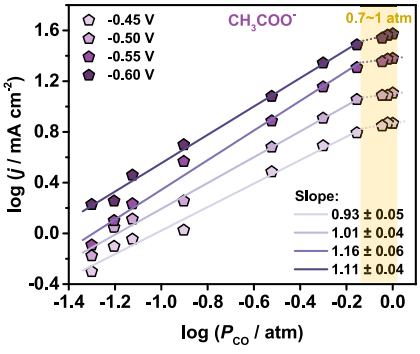

Figure 6. Logarithms of $j_{CH3COO-}$ vs logarithms of P_{CO} at different potentials. Linear fitting is observed at P_{CO} between 0.05 and 0.7 atm.

4. CONCLUSIONS

In summary, reaction kinetic analyses with respect to CO partial pressure allow us to get insight into the possible RDS for CORR toward different C_{2+} products. The similar reaction order trend indicates that C_2H_4 and C_2H_5OH may share the same *CO dimerization step as the RDS and branch at the late stages. The CORR activity to a single C_{2+} product strongly depends on their specific active sites. Particularly, stronger CO binding sites, such as high-uncoordinated defects on the oxide-derived Cu surface, facilitate the selectivity toward C_2H_5OH. Formation of C_3H_7OH likely involves the *CO trimerization mechanism with the third-order reaction relative to θ_{CO}, where the weaker CO adsorption strength is desired. Although the reported rate laws on P_{CO} might not be uniquely suited to the experimental observations, the *CO hydrogenation step is hypothesized to occur before C−C coupling for CH_3COO^- formation.

Intriguingly, the different P_{CO}-dependent kinetic trends of each C_{2+} product were not observed in previous works employing H-cells, probably due to the distinct reaction environments in a GDE-based flow electrolyzer, such as CO availability, local pH, and solvation effect. The Langmuir isotherm has limitations because it neglects the effect of the adsorbate/adsorbate interaction on the adsorption enthalpy, especially under high θ_{CO} conditions. *Operando* spectroscopy technologies, particularly for flow cell systems with high product formation rates, are demanded to reveal further the connection between P_{CO} and θ_{CO} on the catalyst surface. Nevertheless, our rigorous P_{CO}-dependent kinetic analysis

https://doi.org/10.1021/acs.energyfuels.3c00736
Energy Fuels 2023, 37, 7904−7910

offers an efficient attempt to understand possible reaction pathways, associated RDSs, and intermediate adsorption behaviors for the formation of each C_{2+} product. The insight into the reaction mechanism guides the rational design of advanced catalysts and reaction environments for improved $CO_{(2)}RR$ activity and productivity toward a specific C_{2+} product.

■ ASSOCIATED CONTENT

Supporting Information

The Supporting Information is available free of charge at https://pubs.acs.org/doi/10.1021/acs.energyfuels.3c00736.

Ex situ characterization of Cu-based catalysts, electrochemical CO reduction performances, Tafel slopes, theoretical kinetic derivations, and other kinetic data over oxide-derived Cu (PDF)

■ AUTHOR INFORMATION

Corresponding Author

Jingjie Wu − *Department of Chemical and Environmental Engineering, University of Cincinnati, Cincinnati, Ohio 45221, United States;* orcid.org/0000-0001-6617-0895; Email: jingjie.wu@uc.edu

Authors

Zhengyuan Li − *Department of Chemical and Environmental Engineering, University of Cincinnati, Cincinnati, Ohio 45221, United States*

Tianyu Zhang − *Department of Chemical and Environmental Engineering, University of Cincinnati, Cincinnati, Ohio 45221, United States;* orcid.org/0000-0002-0921-6305

Jithu Raj − *Department of Chemical and Environmental Engineering, University of Cincinnati, Cincinnati, Ohio 45221, United States*

Soumyabrata Roy − *Department of Materials Science and NanoEngineering, Rice University, Houston, Texas 77005, United States;* orcid.org/0000-0003-3540-1341

Complete contact information is available at: https://pubs.acs.org/10.1021/acs.energyfuels.3c00736

Notes

The authors declare no competing financial interest.

■ ACKNOWLEDGMENTS

This work was supported by the National Science Foundation (award no. CBET-2033343).

■ REFERENCES

(1) Nitopi, S.; Bertheussen, E.; Scott, S. B.; Liu, X.; Engstfeld, A. K.; Horch, S.; Seger, B.; Stephens, I. E. L.; Chan, K.; Hahn, C.; Nørskov, J. K.; Jaramillo, T. F.; Chorkendorff, I. Progress and Perspectives of Electrochemical CO2 Reduction on Copper in Aqueous Electrolyte. *Chem. Rev.* **2019**, *119*, 7610−7672.

(2) Bagger, A.; Ju, W.; Varela, A. S.; Strasser, P.; Rossmeisl, J. Electrochemical CO2 Reduction: A Classification Problem. *ChemPhysChem* **2017**, *18*, 3266−3273.

(3) Birdja, Y. Y.; Pérez-Gallent, E.; Figueiredo, M. C.; Göttle, A. J.; Calle-Vallejo, F.; Koper, M. T. M. Advances and Challenges in Understanding the Electrocatalytic Conversion of Carbon Dioxide to Fuels. *Nat. Energy* **2019**, *4*, 732−745.

(4) Liu, X.; Schlexer, P.; Xiao, J.; Ji, Y.; Wang, L.; Sandberg, R. B.; Tang, M.; Brown, K. S.; Peng, H.; Ringe, S.; Hahn, C.; Jaramillo, T. F.; Nørskov, J. K.; Chan, K. PH Effects on the Electrochemical Reduction of CO(2) towards C2 Products on Stepped Copper. *Nat. Commun.* **2019**, *10*, 32.

(5) Xiao, H.; Cheng, T.; Goddard, W. A., III; Sundararaman, R. Mechanistic Explanation of the PH Dependence and Onset Potentials for Hydrocarbon Products from Electrochemical Reduction of CO on Cu (111). *J. Am. Chem. Soc.* **2016**, *138*, 483−486.

(6) Montoya, J. H.; Peterson, A. A.; Nørskov, J. K. Insights into C-C Coupling in CO2 Electroreduction on Copper Electrodes. *ChemCatChem* **2013**, *5*, 737−742.

(7) Wang, X.; de Araújo, J. F.; Ju, W.; Bagger, A.; Schmies, H.; Kühl, S.; Rossmeisl, J.; Strasser, P. Mechanistic Reaction Pathways of Enhanced Ethylene Yields during Electroreduction of CO 2 −CO Co-Feeds on Cu and Cu-Tandem Electrocatalysts. *Nat. Nanotechnol.* **2019**, *14*, 1063−1070.

(8) Goodpaster, J. D.; Bell, A. T.; Head-Gordon, M. Identification of Possible Pathways for C−C Bond Formation during Electrochemical Reduction of CO2: New Theoretical Insights from an Improved Electrochemical Model. *J. Phys. Chem. Lett.* **2016**, *7*, 1471−1477.

(9) Garza, A. J.; Bell, A. T.; Head-Gordon, M. Mechanism of CO2 Reduction at Copper Surfaces: Pathways to C2 Products. *ACS Catal.* **2018**, *8*, 1490−1499.

(10) Calle-Vallejo, F.; Koper, M. T. M. Theoretical Considerations on the Electroreduction of CO to C2 Species on Cu(100) Electrodes. *Angew. Chem., Int. Ed.* **2013**, *52*, 7282−7285.

(11) Xiao, H.; Cheng, T.; Goddard, W. A., III Atomistic Mechanisms Underlying Selectivities in C1 and C2 Products from Electrochemical Reduction of CO on Cu(111). *J. Am. Chem. Soc.* **2017**, *139*, 130−136.

(12) Rabinowitz, J. A.; Kanan, M. W. The Future of Low-Temperature Carbon Dioxide Electrolysis Depends on Solving One Basic Problem. *Nat. Commun.* **2020**, *11*, 5231.

(13) Schreier, M.; Yoon, Y.; Jackson, M. N.; Surendranath, Y. Competition between H and CO for Active Sites Governs Copper-Mediated Electrosynthesis of Hydrocarbon Fuels. *Angew. Chem., Int. Ed.* **2018**, *57*, 10221−10225.

(14) Li, J.; Chang, X.; Zhang, H.; Malkani, A. S.; Cheng, M.; Xu, B.; Lu, Q. Electrokinetic and in Situ Spectroscopic Investigations of CO Electrochemical Reduction on Copper. *Nat. Commun.* **2021**, *12*, 3264.

(15) Chang, X.; Li, J.; Xiong, H.; Zhang, H.; Xu, Y.; Xiao, H.; Lu, Q.; Xu, B. C−C Coupling Is Unlikely to Be the Rate-Determining Step in the Formation of C2+ Products in the Copper-Catalyzed Electrochemical Reduction of CO. *Angew. Chem., Int. Ed.* **2022**, *61*, No. e202111167.

(16) Deng, W.; Qiao, Y.; Kastlunger, G.; Govindarajan, N.; Xu, A.; Zhang, P.; Chorkendorff, I.; Seger, B.; Gong, J. Unraveling the Rate-Determine Step of C2+ Products during Electrochemical CO Reductio. *Res. Square* **2023**, DOI: 10.21203/rs.3.rs-2376669/v1.

(17) Verdaguer-Casadevall, A.; Li, C. W.; Johansson, T. P.; Scott, S. B.; McKeown, J. T.; Kumar, M.; Stephens, I. E. L.; Kanan, M. W.; Chorkendorff, I. Probing the Active Surface Sites for CO Reduction on Oxide-Derived Copper Electrocatalysts. *J. Am. Chem. Soc.* **2015**, *137*, 9808−9811.

(18) Feng, X.; Jiang, K.; Fan, S.; Kanan, M. W. A Direct Grain-Boundary-Activity Correlation for CO Electroreduction on Cu Nanoparticles. *ACS Cent. Sci.* **2016**, *2*, 169−174.

(19) Swenson, H.; Stadie, N. P. Langmuir's Theory of Adsorption: A Centennial Review. *Langmuir* **2019**, *35*, 5409−5426.

(20) Wang, L.; Nitopi, S. A.; Bertheussen, E.; Orazov, M.; Morales-Guio, C. G.; Liu, X.; Higgins, D. C.; Chan, K.; Nørskov, J. K.; Hahn, C.; Jaramillo, T. F. Electrochemical Carbon Monoxide Reduction on Polycrystalline Copper: Effects of Potential, Pressure, and PH on Selectivity toward Multicarbon and Oxygenated Products. *ACS Catal.* **2018**, *8*, 7445−7454.

(21) Li, J.; Wang, Z.; McCallum, C.; Xu, Y.; Li, F.; Wang, Y.; Gabardo, C. M.; Dinh, C.-T.; Zhuang, T.-T.; Wang, L.; Howe, J. Y.; Ren, Y.; Sargent, E. H.; Sinton, D. Constraining CO Coverage on Copper Promotes High-Efficiency Ethylene Electroproduction. *Nat. Catal.* **2019**, *2*, 1124−1131.

(22) Lum, Y.; Ager, J. W. Evidence for Product-Specific Active Sites on Oxide-Derived Cu Catalysts for Electrochemical CO2 Reduction. *Nat. Catal.* **2019**, *2*, 86−93.
(23) Cheng, D.; Zhao, Z.-J.; Zhang, G.; Yang, P.; Li, L.; Gao, H.; Liu, S.; Chang, X.; Chen, S.; Wang, T.; Ozin, G. A.; Liu, Z.; Gong, J. The Nature of Active Sites for Carbon Dioxide Electroreduction over Oxide-Derived Copper Catalysts. *Nat. Commun.* **2021**, *12*, 395.
(24) Piqué, O.; Viñes, F.; Illas, F.; Calle-Vallejo, F. Elucidating the Structure of Ethanol-Producing Active Sites at Oxide-Derived Cu Electrocatalysts. *ACS Catal.* **2020**, *10*, 10488−10494.
(25) Kuhl, K. P.; Cave, E. R.; Abram, D. N.; Jaramillo, T. F. New Insights into the Electrochemical Reduction of Carbon Dioxide on Metallic Copper Surfaces. *Energy Environ. Sci.* **2012**, *5*, 7050−7059.
(26) Chen, L.; Tang, C.; Zheng, Y.; Skúlason, E.; Jiao, Y. C3 Production from CO2 Reduction by Concerted *CO Trimerization on a Single-Atom Alloy Catalyst. *J. Mater. Chem. A* **2022**, *10*, 5998−6006.
(27) Fu, X.; Wang, Y.; Shen, H.; Yu, Y.; Xu, F.; Zhou, G.; Xie, W.; Qin, R.; Dun, C.; Pao, C.-W.; Chen, J.-L.; Liu, Y.; Guo, J.; Yue, Q.; Urban, J. J.; Wang, C.; Kang, Y. Chemical Upgrade of Carbon Monoxide to Acetate on an Atomically Dispersed Copper Catalyst via CO-Insertion. *Mater. Today Phys.* **2021**, *19*, No. 100418.
(28) Shen, H.; Wang, Y.; Chakraborty, T.; Zhou, G.; Wang, C.; Fu, X.; Wang, Y.; Zhang, J.; Li, C.; Xu, F.; Cao, L.; Mueller, T.; Wang, C. Asymmetrical C−C Coupling for Electroreduction of CO on Bimetallic Cu−Pd Catalysts. *ACS Catal.* **2022**, *12*, 5275−5283.
(29) Lu, X.; Shinagawa, T.; Takanabe, K. Product Distribution Control Guided by a Microkinetic Analysis for CO Reduction at High-Flux Electrocatalysis Using Gas-Diffusion Cu Electrodes. *ACS Catal.* **2023**, *13*, 1791−1803.
(30) Luc, W.; Fu, X.; Shi, J.; Lv, J.-J.; Jouny, M.; Ko, B. H.; Xu, Y.; Tu, Q.; Hu, X.; Wu, J.; Yue, Q.; Liu, Y.; Jiao, F.; Kang, Y. Two-Dimensional Copper Nanosheets for Electrochemical Reduction of Carbon Monoxide to Acetate. *Nat. Catal.* **2019**, *2*, 423−430.
(31) Heenen, H. H.; Shin, H.; Kastlunger, G.; Overa, S.; Gauthier, J. A.; Jiao, F.; Chan, K. The Mechanism for Acetate Formation in Electrochemical CO(2) Reduction on Cu: Selectivity with Potential, PH, and Nanostructuring. *Energy Environ. Sci.* **2022**, *15*, 3978−3990.

https://doi.org/10.1021/acs.energyfuels.3c00736
Energy Fuels 2023, 37, 7904−7910